Materials and Design 179 (2019) 107897

Contents lists available at ScienceDirect

Materials and Design

journal homepage: www.elsevier.com/locate/matdes

Organic vapor sensing behavior of polycarbonate/polystyrene/multi-walled carbon nanotube blend composites with different microstructures

Yilong Li [a,b], Jürgen Pionteck [a], Petra Pötschke [a,*], Brigitte Voit [a,b]

[a] Leibniz Institute of Polymer Research Dresden (IPF), Hohe Str. 6, 01069 Dresden, Germany
[b] Technische Universität Dresden, Organic Chemistry of Polymers, 01062 Dresden, Germany

HIGHLIGHTS

- Vapor sensing response of immiscible conductive polymer blend composites was studied using different solvents
- The response of composites with 0.75 wt% MWCNT reached up to 1200% after 100 s immersion in saturated ethyl acetate vapor
- At given filler content, vapor sensing depends on the blend morphology type and the polymer-vapor interaction
- Sea-island structures show high resistance changes but poor reversibility, which is opposite for co-continuous structures
- The varied sensing behavior is caused by changed solvent vapor accessibility in different morphology types

GRAPHICAL ABSTRACT

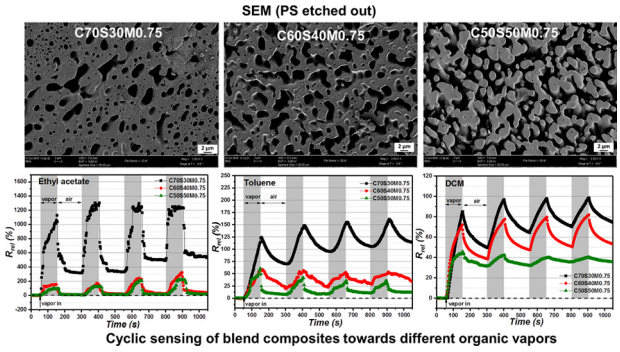

Cyclic sensing of blend composites towards different organic vapors

ARTICLE INFO

Article history:
Received 17 April 2019
Received in revised form 24 May 2019
Accepted 27 May 2019
Available online 28 May 2019

Keywords:
Polymer-matrix composites (PMCs)
Polymer blends
Electrical properties
Vapor sensing
Microstructural analysis
Melt processing

ABSTRACT

With the focus on the use as leakage detectors, the vapor sensing behavior of conductive polymer composites (CPCs) based on polycarbonate/polystyrene/multi-walled carbon nanotube (PC/PS/MWCNT) blends with different blend ratios was studied as well as their morphological and electrical properties. In the melt mixed blend composites, the MWCNTs are preferentially localized in PC. At the PC/PS ratio of 70/30 wt%, the composites showed a sea-island structure, while for blends containing 40 wt% or 50 wt% PS co-continuous structures were developed resulting in a reduction in the MWCNT percolation threshold. The saturated vapors of the selected solvents have good interactions to PS but different interactions to PC. At 0.75 wt% MWCNT, sea-island CPCs showed high relative resistance change (R_{rel}) but poor reversibility towards moderate vapors like ethyl acetate and toluene, while CPCs with co-continuous structure exhibited lower R_{rel} and better reversibility. All CPCs showed poor reversibility towards vapor of the good solvent dichloromethane due to strong interactions between polymers and vapor. In the vapor of the poor solvent cyclohexane, CPCs with higher PS content showed increased R_{rel}. After extraction of the PS component by cyclohexane, the sensing response was decreased and the R_{rel} of the co-continuous blend even reached negative values.

* Corresponding author.
E-mail address: poe@ipfdd.de (P. Pötschke).

https://doi.org/10.1016/j.matdes.2019.107897

1. Introduction

In connection with the protection of the environment and humans, sensing of different kinds of chemical vapors is of increasing importance. At the moment, four material kinds of vapor sensors are widely investigated and reported; namely semiconducting metal oxide sensors (MO) [1,2], conjugated polymer sensors [3], carbonaceous nanomaterial based sensors [4], and sensors based on conductive polymer composites (CPCs) [5–7]. Due to their unique component systems, the different sensor types are based on different sensing mechanisms resulting in different potential application ranges. For instance, for MO based sensors the sensing signal is derived from the electron transfer from the electrode to the MO layer. They exhibit excellent sensitivity at extremely low vapor concentration such as ppm level. However, they are only applicable for a small group of gases such as hydrogen, nitrogen dioxide, etc. For carbonaceous sensor materials, the resistance change results from the adsorption of vapor molecules onto the surface of nanoparticles. They can also detect the vapor concentration at extremely low ppm level because of their thin deposition layer on the interdigital electrode. The sensing mechanism for conjugated polymer sensors is their π-electron delocalization enabling reaction with vapor analytes. However, poor stability and complex processing procedures confine their practical application.

In recent decades, vapor sensors based on CPCs have attracted much attention due to their potential applications in environmental monitoring [8–10], human health detecting [11], or chemical process controlling [12]. CPCs result from the addition of conductive fillers to insulating polymer matrices whereby the fillers form an electrically conductive network within the matrix. The conductive networks are susceptible to external stimuli, such as mechanical [13–17], chemical [9,18,19], electromagnetic [20–23], etc. by changing their electrical resistance. For CPC based vapor sensors, the detected electrical resistance changes result from the disconnection and reconstruction of the conductive network structure caused by polymer swelling and/or by vapor sorption/desorption on the filler surface when the CPC is exposed to such vapors interacting with the polymer matrix. By the matrix swelling the resistance increases and conformational changes of the polymer chains take place. The advantage of this class of materials is the easy fabrication, flexibility in sensor material shape, low costs, fast response, and tunable conductivity and sensitivity. CPC based vapor sensors have been reported to cover a wide analyte detection range over organic chemicals [11,24,25]. The main target of CPC based vapor sensors is to detect vapor leakages and the vapor detection typically occurs in high or saturated concentrations. In industrial applications this concerns leakage problems e.g. in pipes, tanks, landfill sides etc. However, also applications in human health monitoring are reported [11, 26].

Carbon nanotubes (CNTs), especially multi-walled CNTs (MWCNTs), are the most commonly used conductive fillers in such CPCs. In addition to CNTs, carbon black (CB) or graphene-like materials are also applied. The detection of volatile organic compounds (VOCs) is one of the main objectives of CPC based vapor sensors, as VOCs have negative effects on the environment and human health. Feller et al. reported the sensing behavior of a series of CPCs towards different VOCs [27–29]. They investigated conductive biopolymer based composite transducers made of chitosan and CNTs and showed that this type of sensor can be used to detect polar VOCs. In addition, the relative resistance change (R_{rel}) of the sensors showed a positive correlation with an exponential law to the inverse of the Flory-Huggins interaction parameter χ_{12} between the polymer and the vapor [28,30]. Fan et al. immersed thermoplastic polyurethane (TPU) multifilaments into MWCNT dispersions to prepare TPU/CNT core-shell fibers [7]. They discussed the influence of MWCNT content, vapor concentration, and vapor polarity on the final sensor performances of CPCs and demonstrated that such multifilament composites have good reproducibility and fast response to target VOCs. Qi et al. investigated cellulose/MWCNT and cellulose/graphene/aerogel composites and their vapor sensing behavior [5,31]. Compared to solid CPC sensors, these porous aerogel composites showed a faster response, higher sensitivity, and excellent reproducibility to vapors. They also concluded that the dominant sensing mechanism of such porous CNT-cellulose aerogel sensors is the adsorption of vapor molecules on the available free CNT surfaces which increases the distance between the individual nanotubes [21]. In addition to thermoplastic polymer based CPC vapor sensors, thermosetting polymer based sensors were also studied. Mondal et al. investigated the vapor sensing behavior of poly (dimethylsiloxane) (PDMS) filled with CNTs and CB at exposure to hazardous aromatic hydrocarbon vapors [9]. The addition of CNTs influenced the CB dispersion in the PDMS matrix and thus improved the electrical conductivity of the composites. Furthermore, this hybrid filler system was effective in VOC detection and extended the detection range towards different VOCs.

Electrical percolation is a prerequisite for CPCs and the percolation threshold (φ_c) is described as the critical conductive filler amount that leads to the insulator/conductor transition of CPCs. At this composition, a conductive network is formed throughout the entire composite. It has been reported that the sensing behavior of CPCs is related to the structure of the conductive network of CPCs [32]. CPC sensors whose filler content is only slightly higher than φ_c are more sensitive than CPCs whose filler loading is significantly higher than φ_c. A just formed conductive network at lower loadings is more susceptible to external stimuli than a denser network at higher loading. In order to achieve low φ_c, two strategies are commonly utilized. One is the selection of high aspect ratio carbon fillers (CNTs) or large surface area carbon fillers (graphene). For instance, CNTs are widely used as nanofillers due to their extraordinary high elastic modulus, strength, and resilience [33]. Small amount of CNTs can significantly enhance the electrical and mechanical properties of CPCs [34,35]. Liu et al. fabricated thermoplastic polyurethane (TPU)/graphene nanocomposites by the solution-flocculation technique and achieved low φ_c of 0.1 wt%, which indicated that the graphene is a suitable carbonaceous filler to fabricate CPCs with excellent electrical properties [36]. Another strategy to reduce φ_c is to fabricate segregated structures, e.g. through the concept of double percolation. Such structures can be formed in immiscible polymer blends if the filler localizes in a continuous blend component or at a continuous interface of blends. This effect takes advantage from the fact that most carbonaceous fillers have a thermodynamic preference to one of the polymer components and localize there. In co-continuous structures, less filler is needed to make CPCs conductive as only in one of the continuous blend components a conductive network must be formed. This reduces φ_c of such CPCs significantly [37–39]. Zhu et al. designed polystyrene/poly(methyl methacrylate)/MWCNT (PS/PMMA/MWCNT) composites with ultralow φ_c (0.017 wt%) by incorporating MWCNT with carboxyl functional group [37]. These MWCNT were localized at the interface of PS/PMMA, which was attributed to the balance of π-π interactions between PS and MWCNT surfaces and dipole-dipole interactions between PMMA and MWCNT carboxylic groups. Hoseini et al. investigated the electrical conductivity of polystyrene (PS)/polyamide-6 (PA6)/MWCNT composites with different blend morphologies [40]. A co-continuous structure was formed when the PS/PA6 blend ratio was 50/50 wt% resulting in a higher electrical conductivity than that of PA6/MWCNT composites with the same MWCNT loading. MWCNT were preferentially distributed in the PA6 component, which further formed a double percolation network in polymer blends at less filler content.

Up to now, many polymer based vapor sensors have been investigated, but only a few studies have been carried out on vapor sensors based on CPCs based on immiscible polymer blends. In a recently published study, Li et al. prepared poly(lactic acid)/polypropylene/MWCNT (PLA/PP/MWCNT) composites and used different blend ratios [41]. It was found that CPCs with high PLA content displayed a higher R_{rel} to dichloromethane vapor, which is a good solvent to PLA. Similarly, CPCs with high PP content exhibited a higher R_{rel} towards xylene vapor, which is good solvent to PP. In another example, Gao et al. fabricated

polyurethane (PU)/polystyrene-*block*-poly(ethylene-*co*-butylene)-*block*-polystyrene (SEBS)/carbon nanofiber mats via electrospinning [42]. Due to the existence of polar PU and non-polar SEBS, the CPC nanofiber mats were sensitive to both polar and non-polar vapors and showed excellent reversibility. These examples show that the use of blend systems is a promising method to tune the sensitivity and extent the detectable vapor analyte range.

In this work, PC/PS/MWCNT composites with different polymer blend ratios were fabricated by melt processing. In difference to the work on immiscible blends done before, here as polymer blend pair two polymers were selected which show different interactions with the selected acetone, cyclohexane, toluene, ethyl acetate, and dichloromethane (DCM) vapors. For PS all the selected vapors can be regarded as good solvents, whereas for PC acetone and DCM are good solvents, toluene and ethyl acetate are moderate ones and cyclohexane is a poor solvent. The MWCNT dispersion and localization in the polymer blends was analyzed by optical microscopy and scanning electron microscopy. The vapor sensing behavior of the CPCs was investigated by cyclic exposure to the chosen vapors and dry air. The effect of the blend morphology, which depends on the blend component ratio, on the vapor sensitivity of CPCs to various organic vapors was discussed in detail.

2. Materials and methods

2.1. Materials

Polycarbonate (PC) (Makrolon 3108) with a density of 1.2 $g \cdot cm^{-3}$ was purchased from Bayer MaterialScience AG, Germany. Polystyrene (PS) (145D) with a density of 1.05 $g \cdot cm^{-3}$ was received from BASF chemical company, Germany. Multi-walled carbon nanotubes (MWCNT, type NC3100™) with an average length of ca. 1.5 μm and an average diameter of 9.5 nm were obtained from Nanocyl S.A., Belgium. Acetone, DCM, toluene, cyclohexane, and ethyl acetate were obtained from Sigma-Aldrich, Germany. All chemicals were used as received.

2.2. Sample preparation

The PC/PS/MWCNT composites were fabricated in a single-step mixing process using a twin-screw micro-compounder with a capacity of 15 cm^3 (Xplore, The Netherlands) at 240 °C for 5 min; the rotation speed was 250 rpm. Prior to compounding, PLA and PS granules and MWCNT were dried in a vacuum oven at 60 °C for 16 h to remove trace water. PLA/PS blends with different blend ratios (70/30 wt%, 60/40 wt% and 50/50 wt%) without and with MWCNTs were processed. The obtained extruded strands were pelletized and then compression molded (240 °C, 20 kN for 5 min) into circular plates (diameter of 60 mm and thickness of 0.3 mm) using a hot press machine (PW40EH, Paul Weber GmbH, Germany). For the vapor sensing tests, rectangular samples ($10 \times 5 \times 0.3$ mm^3) were cut from the circular plates.

The PC/PS/MWCNT composites with different polymer blend ratios and filler contents are denoted as C*x*S*y*M*z*, where *x*, *y*, and *z* represent the weight fraction of PC, PS, and MWCNT, respectively. C50S50M0.75 means that the PC/PS blend ratio is 50/50 wt%, and the MWCNT loading is 0.75 wt%. For the sensing tests, samples with 0.75 wt% MWCNTs were selected, which corresponds to a MWCNT content related to the PC part of the blends of 1.07 wt% (C70S30), 1.25 wt% (C60S40) and 1.50 wt% (C50S50). For selected sensing experiments, the PS component was extracted from the blend composites using cyclohexane. For this, compression molded samples were immersed in cyclohexane for 48 h at room temperature. After extraction, the samples were rinsed by cyclohexane and dried in a vacuum oven at 60 °C. The extracted samples are denoted as E-C*x*S*y*M*z*.

2.3. Characterization

2.3.1. Electrical resistivity measurements

The electrical volume resistivity measurements were performed on the pressed circular plates. Generally, plate samples whose resistivity was higher than 10^7 Ω·cm were measured using a Keithley electrometer 6517A together with a Keithley 8009 resistivity test fixture equipped with ring electrodes (both from Keithley Instruments Inc., USA). If the resistivity was lower than 10^7 Ω·cm, the measurement was performed on strips (cut from the circular plates) with the dimension of $30 \times 5 \times 0.3$ mm^3 using a 2-point test fixture connected to the Keithley DMM 2000 electrometer (Keithley Instruments Inc., USA). At least 4 strips were measured per sample to calculate the mean value and the standard deviation. It should be noted that a MWCNT density of 2.1 $g \cdot cm^{-3}$ [43] was used for the calculation of MWCNT vol% for fitting of the electrical percolation threshold of the CPCs. The electrical conductivity values calculated from the resistivity values were non-linearly fitted according to the well-known and typically used Eq. (1)

$$\sigma = \sigma_0(\varphi - \varphi_c)^t \quad (1)$$

where σ represents the conductivity of the composite with different filler loadings, φ and φ_c are the filler volume content and the percolation threshold, respectively, and t is an exponent used to explain the formation mechanism of the conductive networks. The fitting was done with conductivity values above φ_c as below φ_c not enough measurement points were available. With the origin8.0 software, φ_c was varied in steps of 0.01, starting from an estimated φ_c value, until the lowest value of the mean square error to the measured conductivity values was obtained [43].

2.3.2. Morphological characterization

The macro-dispersion of MWCNTs in the polymer blends was evaluated by transmission light microscopy (TLM). MWCNT materials are typically produced in agglomerated shape [44] due to the strong Van der Waals forces among the single tubes that make them easily entangled with each other. During melt mixing, dispersion, meaning individualization of the primary agglomerates into single tubes, is difficult to achieve [45] and the state of the achieved macro-dispersion under the selected mixing conditions was therefore assessed using TLM. Thin sections with a thickness of 5 μm were cut from the extruded strands using a Leica RM2265 microtome (Leica Microsystems GmbH, Germany). Images were taken with a BH2 microscope equipped with a DP71 camera (Olympus Deutschland GmbH, Germany). The amount of remaining agglomerates, seen as dark areas in the transmission images, was analyzed from TLM images by means of the OLYMPUS Stream Image Analysis Software (Bethesda, USA). The agglomerate area ratio ($A_{Agg} = A/A_0$) is defined as the ratio of the area of MWCNT agglomerates (with a circle-equivalent diameter > 5 μm) (A) to the total area of the image (A_0). For sufficient statistical accuracy, at least 15 images were taken and evaluated from each sample.

To assess the blend morphology and MWCNT localization, scanning electron microscopy (SEM) characterization was performed on cross-sections of extruded CPC strands by anULTRA-55 (Carl Zeiss AG, Germany) with an accelerating voltage of 3 kV. Fractured strands were smoothed using the Leica RM2265 microtome at room temperature. To better visualize the blend morphology, PS was extracted by dipping the PC/PS/MWCNT strand pieces into cyclohexane at room temperature for 6 h. Then these etched specimens were washed with cyclohexane in an ultrasonic bath for another 15 min. The cut and etched sample surface was sputter coated with platinum to avoid electrostatic charging during the SEM analysis. Images at lower magnification were used to assess the blend morphology and those taken at higher magnifications to analyze the MWCNT localization and micro-dispersion.

2.3.3. Estimation of PS continuity by solvent extraction

Solvent extraction is used to obtain information about the continuity of the PS component in the blends. For the extraction experiments, the extruded strand samples were cut along the extrusion direction, whereby the cross-sectional area along the extrusion direction is approx. 1 cm^2 (length of 2 cm and width of 0.5 cm). Then the samples were immersed in cyclohexane for 48 h at room temperature to selectively extract the PS component from the blend. After extraction, the samples were rinsed by cyclohexane and dried in a vacuum oven at 60 °C for another 3 h. The extracted PS content of CPCs is calculated based on the initial mass and the change in the mass of the composites after extraction using Eq. (2). [46]

$$\varphi_i = \frac{m_0 - m_i}{m_0} \times 100\% \quad (2)$$

where φ_i is the extracted component content of the CPC, m_0 is the initial mass of the CPC and m_i is the remaining mass of the CPC after extraction.

2.3.4. Vapor sensing tests

The vapor sensing behavior of CPCs was investigated by in-situ recording the electrical resistance changes R_{rel} of the CPCs during several successive immersion-drying runs (IDRs). The two ends of the strip samples were covered with silver paste to ensure good contact between the specimens and the electrodes. The setup for vapor sensing is schematically shown in Fig. S1, which has been presented in our previous work [32]. This self-made set-up was connected with a digital multimeter (Keithley 2400, USA) to record the electrical resistance of the samples. The R_{rel} is normalized using Eq. (3).

$$R_{rel} = \frac{R - R_0}{R_0} \times 100\% \quad (3)$$

where R_0 and R are the initial resistance and the actual resistance of the samples, respectively. To ensure exact vapor concentrations, a bubbler evaporation system was applied to deliver controlled vapor amounts to the detection chamber (25 mL) using dry air as carrier and diluent for the vapors. The maximum gas flow rate was set as 30 L/h by manipulating the vapor flow controller and air flow controller during the measurement, thus the vapor concentration can be calculated by Eq. (4).

$$C = \frac{P_i}{P} \times \frac{f}{(f+F)} \times 100 \quad (4)$$

where P is the input air pressure, and P_i is the saturated partial pressure of organic solvent at 25 °C. F and f represent the air flow rate and vapor flow rate, respectively. Atmospheric pressure is applied in all tests and the temperature is 25 °C. The sensing protocol for the successive cyclic sensing is 100 s exposure and 150 s drying of each cycle. For the characterization of the sensitivity of the materials versus acetone vapor, different acetone vapor concentrations were applied and the mean values and standard deviation among the 4 IDRs were calculated. For each vapor concentration, a new sample was used. For the long-term immersion experiment, the samples are exposed for 500 s in the corresponding vapor.

3. Results and discussion

3.1. Electrical properties and morphological observations of PC/PS/MWCNT blend composites

Fig. 1 shows the volume conductivity of the different PC/PS/MWCNT blend composites as a function of MWCNT volume content. For C70S30 (Fig. 1a), there is a sharp conductivity increase by 10 orders of magnitudes when the MWCNT loading increases from 0.25 wt% to 0.5 wt% (corresponding to 0.14 vol% to 0.29 vol%), which indicates the formation of a conductive network. C60S40 (Fig. 1b) and C50S50 (Fig. 1c) exhibit a similar electrical percolation at much lower MWCNT contents as compared to C70S30 composites. Based on Eq. (1), the φ_c of C70S30M*z* was fitted to be 0.30 vol%. With the increase of the PS content in the blend, the φ_c decreases to 0.15 vol% for C60S40M*z* and 0.13 vol% for C50S50M*z* blend composites. At 0.75 wt% MWCNTs (approx. 0.43 vol %), the content used for the following sensing tests, the electrical conductivity values are 6.5×10^{-4} S·cm^{-1} for C70S30, 5.9×10^{-4} S·cm^{-1} for C60S40, and 1.2×10^{-4} S·cm^{-1} for C50S50M. This indicates that although the C70S30 based sample is closer to the corresponding percolation threshold it has the highest conductivity value compared to the other two samples. The highest conductivity despite the lowest MWCNT content related to the PC part (1.07 wt% MWCNT related to PC) can be explained by the blend morphology as discussed below.

Transmission light micrographs of thin sections of the blend composite with 0.75 wt% MWCNT are shown in Fig. 2. In these samples, primary MWCNT agglomerates are still present under the selected mixing conditions, suggesting that a part of the MWCNT material has not effectively contributed to the formation of the electrically conductive network. The MWCNT agglomerate area ratio A_{Agg} increases with rising PS and decreasing PC content in the blends. For example, the A_{Agg} of C70S30M0.75 is 0.65%, while the values for C60S40M0.75 and C50S50M0.75 are 1.56% and 2.19%, respectively. These are 2.4 and 3.4 times greater than the value of C70S30M0.75, respectively. It can be deduced that MWCNTs have a better dispersion in PC/PS blend with high PC content, in which the filler content related to the PC part is lower.

Fig. 3 presents the SEM micrographs of PC/PS/MWCNT-0.75 wt% strand cross-sections. The smoothed fracture surfaces of the strands were immersed in cyclohexane to extract the PS component. For C70S30M0.75, it can be observed that the PS component, which appears as holes after extraction, forms some spherical particles embedded in the PC matrix, which is characteristic for a sea-island structure (Fig. 3a–c). At higher magnification (Fig. 3c), it can be seen that the MWCNTs are localized in the PC matrix, which is in accordance with the thermodynamic prediction (see Tables S1–S3). For C60S40M0.75 (Fig. 3d), the composite morphology is quite different from that of C70S30M0.75. The elongated PS structures have started to connect with each other and form a continuous structure [47]. In overall, PC is still the major component in C60S40M0.75; however, PS is already seen to be partially through going in these cuts. At high magnification (Fig. 3e and f), it can be seen that some individual MWCNTs remain after the etching process on the surface of the PC component. In C50S50M0.75 (Fig. 3g–i), the co-continuity is further evolved. The remained PC component is finer and the co-continuous structure is clearly seen (see Fig. 3g). The co-continuous structure together with the selective localization of the MWCNTs within PC and the attainment of φ_c in the PC part represents the effect of double percolation in CPCs and is the reason for the observed significantly lower φ_c as compared to C70S30 blends. Interestingly, MWCNTs are not only found in the cross-section of remaining PC component but also at the surface of the PC component (e.g. Fig. 3i). This indicates that even if most of the MWCNTs are localized in the PC component, some MWCNTs were expelled to the PC/PS interface because of the relatively low PC content in C50S50M0.75 composites.

Fig. 4 shows the weight loss of CPCs with 0.75 wt% MWCNT caused by PS extraction with cyclohexane. From the strand samples, about 5 wt% of C70S30M0.75 were extracted, which is far lower than the actual PS content of 30 wt% in the blend. Due to the isolated spherical PS domains in the PC matrix, the PS imbedded within the sample is only partially accessible to cyclohexane. For C60S40M0.75, the extracted part increased to 25 wt%, which is still lower than the actual PS content in the blend (40 wt%). From C50S50M0.75 an amount of 40 wt% was extracted, which is only slightly lower than the actual PS content in the blend (50 wt%) and illustrates a nearly perfect co-continuous structure.

The inset photos in Fig. 4 show the cyclohexane solutions after extraction. It can be seen that the solvent becomes more turbid with

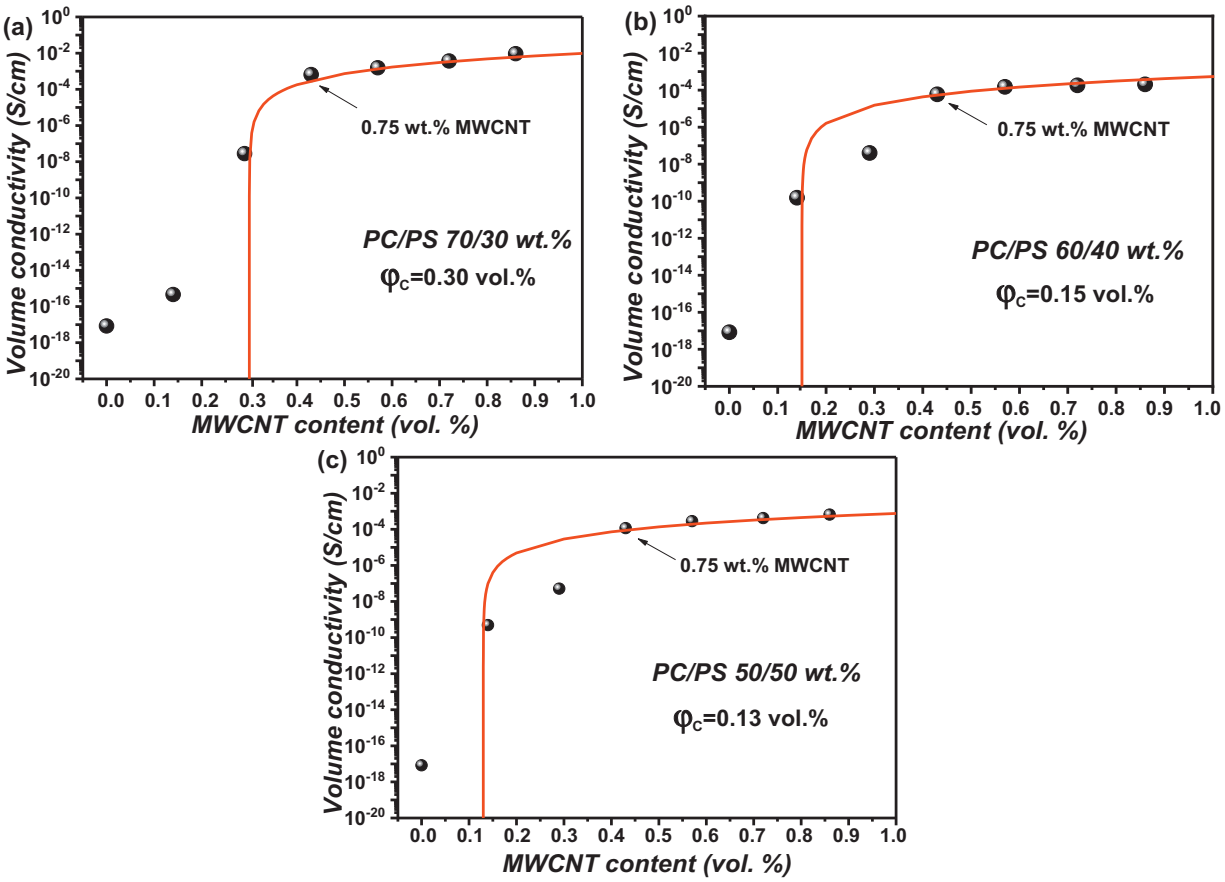

Fig. 1. Electrical conductivity as a function of MWCNT content for PC/PS/MWCNT composites with different PC/PS blend ratios: (a) 70/30 wt%, (b) 60/40 wt%, and (c) 50/50 wt%.

increasing PS content in the blends. Furthermore, the relatively dark extracted solution of C50S50M0.75 shows that obviously some MWCNTs were extracted as well. In this blend, the PC-related MWCNT content is highest (1.5 wt%) and the MWCNT agglomerates are the largest. This also suggests that some MWCNTs may be located in the PS component or near the interface as the filler saturation in the PC component releases the excess MWCNTs to the PS component.

3.2. Vapor sensing behavior of PC/PS/MWCNT blend composites

As reported, the vapor sensing behavior of CPCs is influenced by the filler loading, polymer-vapor interaction, and filler dimensionality [48,49]. However, the effect of composite microstructure on the vapor sensing behavior has not yet been investigated in detail. In this study, five organic solvents namely acetone, ethyl acetate, DCM, toluene and cyclohexane were chosen (see Table 1). The composites C70S30M0.75, C60S40M0.75 and C50S50M0.75 were selected for the vapor sensing studies because their initial resistances and those at solvent vapor exposition were below the upper resistance limit (200 MΩ) of the electrometer used. The interaction between polymer and organic vapor can be estimated by the Flory-Huggins interaction parameter χ_{12}, which is calculated by Eq. (5):

$$\chi_{12} = \frac{V_1^0}{RT}(\delta_1 - \delta_2)^2 \tag{5}$$

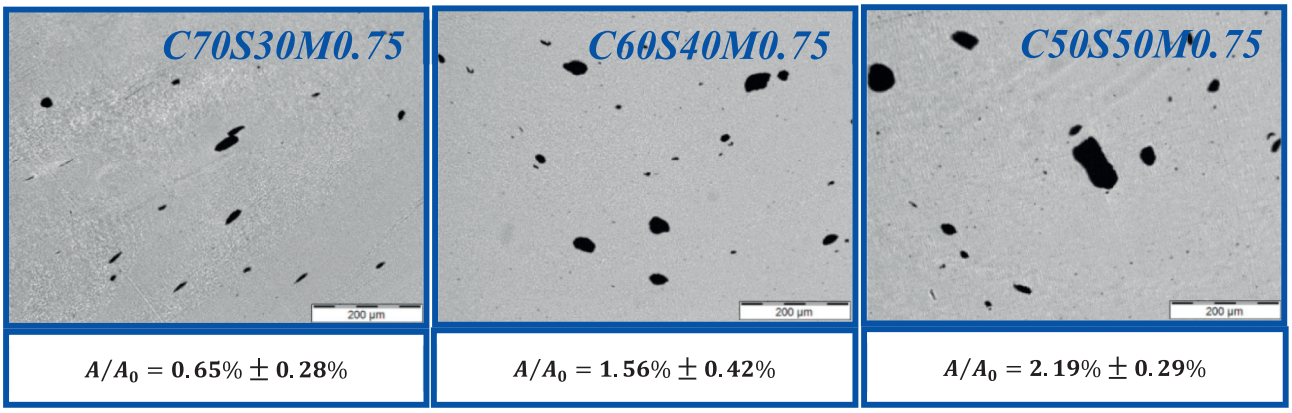

Fig. 2. TLM images of the blend composites with 0.75 wt% MWCNT illustrating the different dispersion states of MWCNTs in the polymer blends.

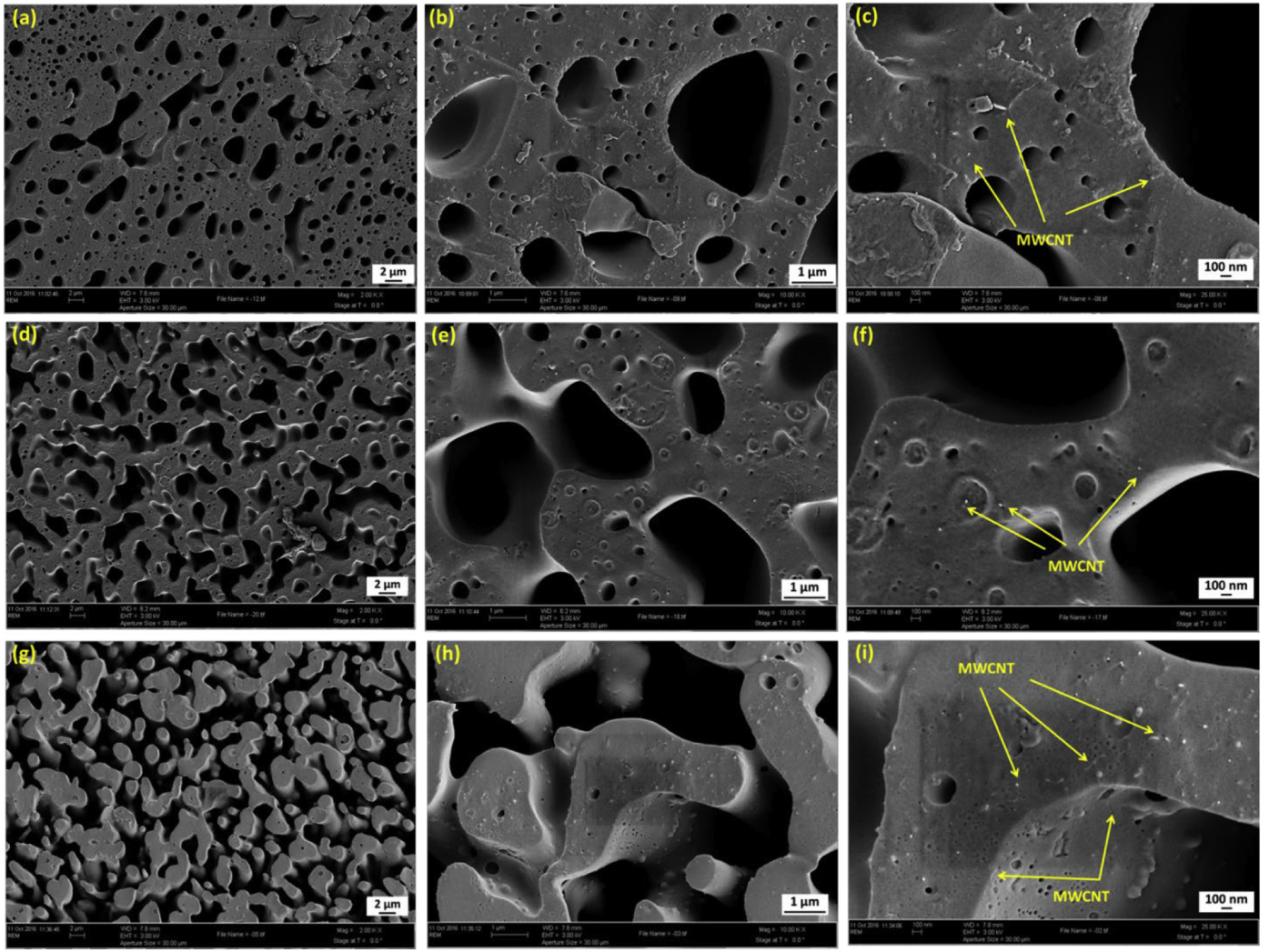

Fig. 3. SEM images of the PC/PS/MWCNTs composites containing 0.75 wt% MWCNT. (a), (d) and (g) are C70S30M0.75, C60S40M0.75 and C50S50M0.75, respectively, (b, c), (e, f) and (h, i) are higher magnifications of the three composites.

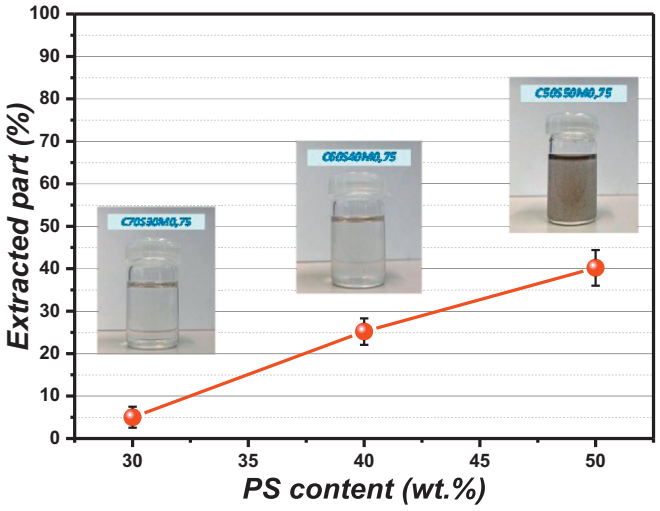

Fig. 4. Extracted part for PC/PS/MWCNT-0.75 wt% with different blend ratios, inset photographs show the cyclohexane solutions after extraction.

In Eq. (5), V_1^0 is the solvent molar volume ($cm^3 \cdot mol^{-1}$), R is the ideal vapor constant (8.314 $J \cdot mol^{-1}$), T is the temperature (K), and δ_1 and δ_2 are the solubility parameters of solvent and polymer ($J^{1/2} \cdot cm^{-3/2}$), respectively. The calculated χ_{12} values between polymers and organic vapors are listed in Table 1. According to the definition of polymer-vapor interaction proposed by Hansen et al. [50], $\chi_{12} < 0.5$ is considered to be a strong polymer-vapor interaction. Thus, it can be concluded from Table 1 that acetone and DCM are good solvents for PC, ethyl acetate and toluene cause moderate swelling of PC, and cyclohexane poorly interacts with PC due to their large χ_{12} value. In terms of PS, the small χ_{12} values suggest that all the selected vapors have good interactions with this polymer. Thus, in this work three different cases can be distinguished according to the different interactions of the selected vapors to PC, namely good interactions (acetone, DCM), moderate interactions (ethyl acetate and toluene), and poor interaction (cyclohexane).

In the beginning of vapor sensing measurement, the samples were immersed in dry air for 50 s to get a stable initial resistance before exposing them to the organic vapors. Then the samples were exposed to four successive cycles of alternating vapor and dry air. Fig. 5a shows the R_{rel} of PC/PS/MWCNT blend composites towards saturated ethyl acetate vapor. When comparing the cyclic sensing curves of the CPCs, it can be observed that C70S30M0.75 has a higher R_{rel} than C60S40M0.75 and C50S50M0.75 composites. For C70S30M0.75 there is a significant R_{rel} increase when the sample is exposed to ethyl acetate vapor and the final R_{rel} of the first cycle after 100 s exposure is approximately 1100%. Afterwards, during the drying period the R_{rel} decreases rapidly and reaches a plateau. However, the R_{rel} does not recover to the initial state and its final value after the first drying is 300%, indicating that the conductive network of CPCs is partially damaged and cannot be fully reconstructed. For C60S40M0.75 and C50S50M0.75 the maximum R_{rel} after the first exposure is only 175% for C60S40M0.75 and 100% for C50S50M0.75. However, these samples show a good reversibility and the R_{rel} values returned to their initial states after the drying time. When comparing the maximum R_{rel} of each cycle for C70S30M0.75, it can be seen that the values are between 1100% and 1300%, which shows that the conductive network in C70S30M0.75 is highly susceptible to polymer swellings when exposed to ethyl acetate vapor. For C60S40M0.75, its maximum R_{rel} shows a slight increase from the first cycle of 150% to the fourth cycle of 325%, and a similar trend is seen for C50S50M0.75, whose R_{rel} is in the range of 100% to 220% during these consecutive sensing cycles. The big difference of sensing behavior of these three CPCs is attributed to the blend microstructure. The higher maximum R_{rel} values at higher PC content result from the localization of a relatively lower MWCNT content in the continuous PC matrix of the sea-island structure. This enables a better accessability of the solvent vapor towards PC resulting in larger swelling and network changes as compared to the co-continuous structure, where the accessability and swelling are more hindered by the as well continuous PS. On the other hand, the co-continuous structure with larger continuous interfaces facilitates the vapor evaporation from the blend matrix [18], which leads to better reversibility compared to the blend composite with sea-island structure.

Fig. 5b shows the cyclic vapor sensing behavior of CPCs towards saturated toluene. Although toluene and ethyl acetate have only slightly different χ_{12} values to PC and PS, the CPCs show a much lower R_{rel} in toluene than in ethyl acetate vapor. For C70S30M0.75 the maximum R_{rel} in the first immersion step reaches 125%, followed by a R_{rel} decrease to about 70% during drying. Based on the results of the C70S30M0.75 cyclic scan curve, the conductive network is gradually damaged with the sensing cycles resulting in poor reversibility. In comparison, the maximum R_{rel} of C60S40M0.75 and C50S50M0.75 show a decreasing tendency with the sensing cycle. First, the maximum R_{rel} of both samples is 60%, in the fourth cycle the R_{rel} of C60S40M0.75 is only 52%, while in C50S50M0.75 it is only 35%. This shows that the toluene vapor penetration makes the conductive network especially of C50S50M0.75 more perfect during the sensor test and thus less sensitive to further cycles.

In summary, it can be concluded that the blend structure of the CPCs plays an important role in vapor sensing of moderate organic vapors such as ethyl acetate and toluene. CPCs with co-continuous structures have a lower R_{rel} due to the following reasons: Because of the selective localization of the CNTs in PC, a lower PC content in the blends leads to a denser conductive network in this component compared to CPCs with higher PC loading and the same MWCNT content. Furthermore, the co-continuous structure has a continuous interface that can facilitates vapor penetration and evaporation during sensor testing resulting in better stability over different cycles. In general, the strong interaction between a polymer and its good solvents results in strong polymer swelling and complete damage of the conductive network. Therefore, CPCs in saturated good solvent vapors always exhibit poor reversibility as the conductive network is irreversibly damaged.

For this reason, the vapor concentration of dichloromethane, a good solvent to PC, was reduced to 23.5% (the saturated vapor concentration is 53.0%) by adjusting the mass flow controllers according to Eq. (3). Fig. 5c shows the cyclic vapor sensing behavior of the CPCs towards DCM vapor. Even though the DCM vapor was diluted, all CPCs show a conditioning effect in the first cycle due to the strong interaction

Table 1
Flory-Huggins interaction parameters χ_{12} of polymers and organic solvents at 25 °C [50].

Materials	V_{mol} ($cm^3 \cdot mol^{-1}$)	Pi (kPa, 25 °C)	δ_D $(MPa)^{1/2}$	δ_P $(MPa)^{1/2}$	δ_H $(MPa)^{1/2}$	δ $(MPa)^{1/2}$	χ_{12}	
							PC	PS
Acetone	74	30.6	15.5	10.4	7.0	19.9	0.003	0.011
Ethyl acetate	98.5	12.6	15.8	5.3	7.2	18.2	0.159	0.048
DCM	67.8	53.0	18.2	6.3	6.1	20.2	0.0003	0.022
Toluene	106.8	3.8	18.0	1.4	2.0	18.2	0.172	0.052
Cyclohexane	130.6	13.0	16.8	0	0.2	16.8	0.507	0.274
Polycarbonate			18.1	5.9	6.9	20.3	–	–
Polystyrene			18.5	4.5	2.9	19.3	–	–

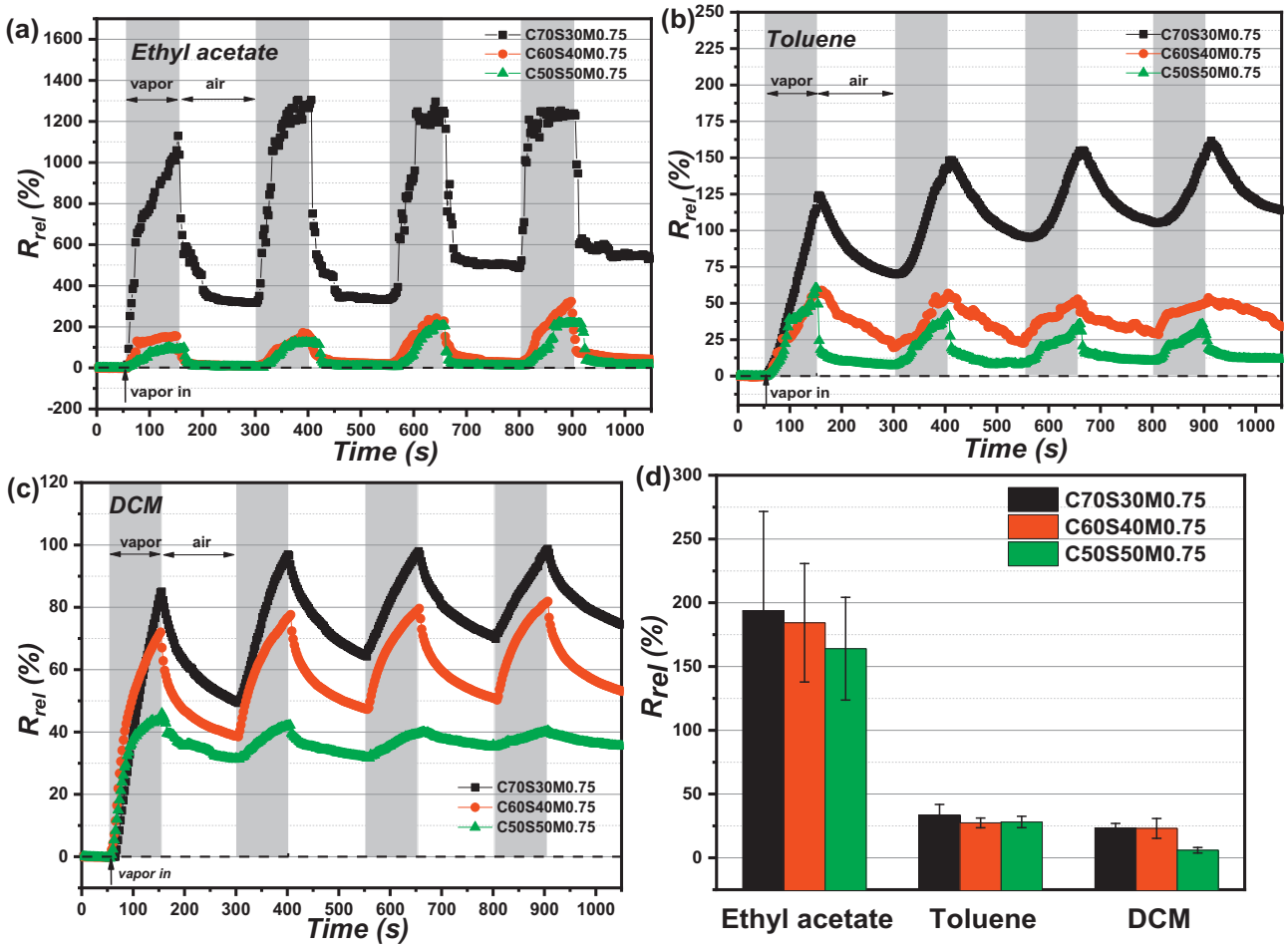

Fig. 5. Cyclic sensing behavior of PC/PS/MWCNT composites with different blend ratios towards (a) saturated ethyl acetate vapor, (b) saturated toluene vapor, (c) diluted DCM vapor (23.5% vapor concentration). (d) Mean values of relative resistance change of CPCs from the second cycle to fourth cycle towards different vapors. R_{rel} is calculated based on the initial resistance value before each cycle, error bars show the standard deviation of the three regarded cycles.

between PC and DCM vapor. Starting with the second cycle, C70S30M0.75 and C60S40M0.75 have a gradually increased maximum R_{rel} with the sampling cycle. The gradually increasing R_{rel} after each immersion and drying cycle also indicates irreversible damage of the conductive network in contact with the good vapor DCM. For C50S50M0.75, R_{rel} and its changes with the cycles have the lowest values. It can therefore be assumed that C50S50M0.75 has the densest conductive network, which is very stable under polymer swelling. In addition, the poor reversibility of CPCs to dichloromethane is due to the strong polymer-vapor interaction, which makes polymer relaxation more difficult.

In general, the stresses generated within the polymer composite during the melt shaping process can relax during the first vapor loading due to the increased mobility of the polymer chains in the swollen state. Thus, the first exposure is considered as conditioning cycle and the following cycles should be regarded. In order to compare the efficiency of sensing, the mean R_{rel} of the regarded cycles (2nd cycle to 4th cycle) of CPCs towards ethyl acetate, toluene and DCM vapors are plotted and shown in Fig. 5d. In this plot, R_{rel} is calculated based on the initial resistance of each cycle and the error bars indicate the standard deviation of the three regarded cycles. It is shown that the mean R_{rel} values of the CPCs for these considered cycles are mainly related to the polymer interaction. CPC sensors have a higher R_{rel} in saturated ethyl acetate vapor than saturated toluene vapor, which corresponds to the polymer-vapor interaction ranking given in Table 1. In addition, the diluted DCM vapor induces a lower R_{rel}, although it exhibits a very strong interaction with the PC. When comparing the R_{rel} of CPCs with different blend ratio, C70S30M0.75 composites always have the highest R_{rel}, followed by C60S40M0.75 and C50S50M0.75, where the difference of the mean R_{rel} is less pronounced.

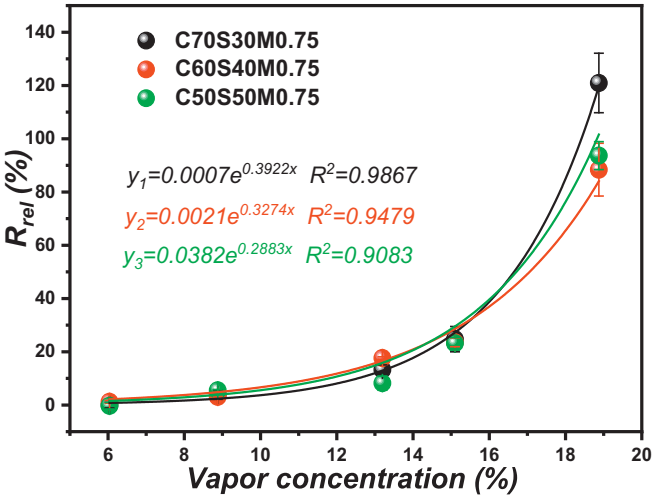

Fig. 6. Relative resistance changes at different acetone vapor concentrations for different composites under dynamic flow conditions. The lines are drawn according to fitting to the exponential fitting model $y = a * e^{bx}$.

To investigate the sensitivity of CPCs towards organic vapors, Fig. 6 illustrates R_{rel} values of CPCs at different acetone vapor concentrations. Acetone is good vapor to both PC and PS components (see Table 1). To fit the data, we applied an exponential model given in Eq. (6) [9].

$$R_{rel} = a * e^{bx} \quad (6)$$

where a and b are constants and x is the vapor concentration. Fig. 6 shows an exponential relationship of the sensor response with the vapor concentration. The R_{rel} values in Fig. 6 represent the mean values and the standard deviation of the maximum R_{rel} of the four exposure/drying cycles. When the vapor concentration is below 15%, all the three kinds of CPCs have almost the same low R_{rel} and the R_{rel} increases only slightly with the increase of acetone vapor concentration. When the vapor concentration is 18.9%, the R_{rel} of CPCs are several times higher than at lower vapor concentrations. In particular, C70S30M0.75 shows the highest R_{rel} at 18.9% acetone vapor concentration compared to the other concentrations, even if this sample has the highest initial conductivity, indicating the best network quality. However, with this blend composition, the selected 0.75 wt% MWCNT loading is closer to the corresponding percolation threshold than with the other blend compositions, leading to the expectation of higher sensitivity of the developed network. In summary, the blend structure in which MWCNTs are dispersed in good quality in the matrix component of the sea-island structure allows better accessibility to vapors and thus reacts more sensitively to the stimulation by good organic solvent vapors at higher vapor concentration. The correlations shown in Fig. 6 can be regarded as calibration curves of the CPC materials, i.e. based on the R_{rel} observed under the same measuring conditions (100 s immersion, room temperature) an unknown acetone vapor concentration (in the range between 6% and 18.9%) can be predicted.

Fig. 7a demonstrates the sensing performance of CPCs for the long-term exposure towards saturated cyclohexane vapor. As discussed above (see Table 1), cyclohexane is a better solvent for PS than for PC. All three CPCs nearly reach an equilibrium state after the long-term exposure (500 s) to cyclohexane vapor, however, the R_{rel} are very low due to the weak interaction between PC and cyclohexane. For C70S30M0.75, its equilibrium R_{rel} is only 1%, and the R_{rel} of C60S40M0.75 and C50S50M0.75 are ca. 3% and 5%, respectively. This is a result of the sorption-desorption behavior of CPCs with different microstructures. For C70S30M0.75, the conductive network variations are mainly resulting from the cyclohexane penetration into the PC matrix that causes the mild swelling of PC. PS is shielded in the sea-island structure from swelling. For C50S50M0.75 however, cyclohexane can penetrate into the PC and the PS components simultaneously. The PS component will be more swollen because of the stronger interaction between PS and cyclohexane. Therefore, the conductive network in the PC component will also be influenced by the PS swelling, thus leading to a higher R_{rel} of C50S50M0.75 compared to C70S30M0.75 when they are exposed to cyclohexane. In addition, for C50S50M0.75 it was suggested from morphological and extraction results that some part of the CNTs is located near the PS/PC interface, thus also contributing more effectively to resistance change.

To further illustrate the effect of PS in polymer blends on the sensing behavior in cyclohexane, the PS part of the CPC samples was extracted using cyclohexane. Fig. 7b shows the sensing curves of the treated CPCs after long-term cyclohexane vapor exposure. Obviously, the extracted CPCs E-C70S30M0.75 and E-C60S40M0.75 show a similar

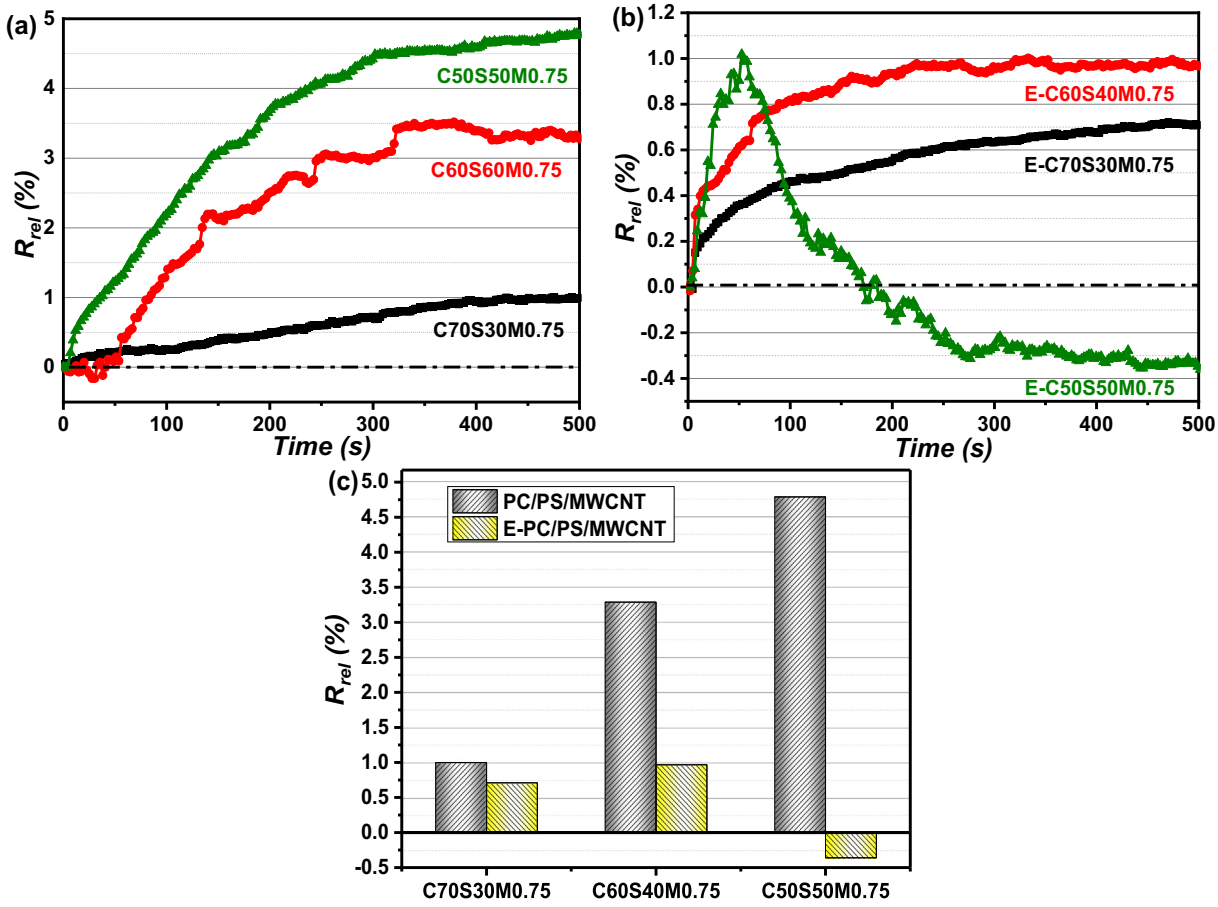

Fig. 7. Long-term immersion in saturated cyclohexane vapor of (a) PC/PS/MWCNT composites and (b) cyclohexane etched PC/PS/MWCNT composites; (c) comparison of terminal R_{rel} of CPCs after 500 s exposure to cyclohexane vapor.

sensing tendency as the untreated samples, but lower R_{rel} values, whereas for E-C50S50M0.75 R_{rel} increases strongly up to the peak value of 1% after 50 s immersion and then it gradually decreases and reaches even negative changes (increase of conductivity). The terminal R_{rel} of solid and extracted CPCs are compared in Fig. 7c. The terminal R_{rel} of the solid CPCs increases with rising PS content, which proves that CPCs with co-continuous structure are more sensitive to the poor solvent vapor because of their microstructure. Interestingly, an obvious terminal R_{rel} distinction is observed for CPCs where PS was extracted before. After extration, E-C70S30M0.75 and E-C60S40M0.75 show lower R_{rel} as compared to the corresponding solid CPCs. This is because the remaining filled PC matrix is not influenced anymore by the swelling of the PS component to cyclohexane and the conductive network can be maintained during vapor exposure. For E-C50S50M0.75, the negative R_{rel} is attributed to the large surface of the open porous structure that promotes the vapor penetration into the PC matrix, which helps to rearrange the MWCNTs in the PC component, even if the interaction between PC and the cyclohexane vapor is low. Possibly an increase in the PC chain mobility by absorbed cyclohexane results in a rearrangement of the conductive network towards a more perfect structure; however this has to be studied in more detail.

A schema is proposed in Fig. 8 to illustrate the difference between the solid and porous structures. Fig. 8a shows the blend microstructure of C70S30M0.75 before and after extraction. This composite has the typical sea-island structure and the MWCNTs are homogeneously distributed in the PC matrix component. After cyclohexane extraction, isolated PS domains are partially extracted but the conductive network is still present due to the weak interaction of PC and cyclohexane. For C50S50M0.75 composites (see Fig. 8b), the major part of the PS component has been extracted by cyclohexane due to its continuous structure. In this process, some MWCNTs distributed near the PC/PS interface or even in PS are also extracted, which partially breaks the conductive network in the composite material. When this material now is exposed to cyclohexane vapor, the low swelling of the PC causes a stronger initial increase of resistance. Parallel to that the cyclohexane diffuses into the PC part, increases the chain mobility and enables a rearrangement of the conductive network, leading to a decrease in resistance of E-C50S50M0.75.

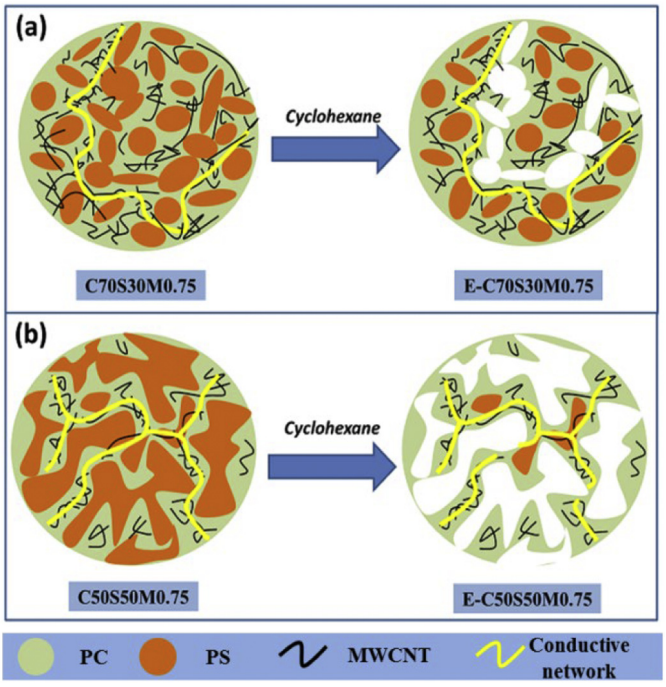

Fig. 8. Schematic of morphology changes and MWCNT distribution of PC/PS/MWCNT composites after extraction by cyclohexane; (a) C70S30M0.75 composites and (b) C50S50M0.75 composites.

As a summary, when exposed to solvent vapors CPCs based on immiscible polymer blends lead to more diverse electrical resistance changes than CPCs based on single polymers [32]. According to the discussion above, CPCs with co-continuous structure improve the reversibility to good vapors and prolong the lifespan of sensor materials. Moreover, they are also sensory to poor vapors that broaden the detectable analyte ranges for sensing tests. The vapor sensing behavior of CPCs can be tuned by adjusting the blend structure and filler distribution state of CPCs.

4. Conclusions

This study describes the vapor sensing behavior of immiscible polymer blend based CPCs at a given filler content, which is not only determined by the interaction of the blend components with specific solvents, but also by the blend morphology type. This is related to the accessability of the solvent vapor to the blend components which is determined by the blend morphology. Different blend morphology types were achieved by varying the polymer blend ratio when melt-mixing PC with PS and the morphological and electrical properties of the composites at different MWCNT contents were studied. The MWCNTs are preferably localized in the PC component according to the thermodynamic calculation, which corresponds to the morphological findings. The percolation threshold of the composites with co-continuous structure (PC/PS 50/50 wt%) is 0.13 vol%, which is lower than that of 0.30 vol% of the composites with sea-island structure (PC/PS 70/30 wt %). The sensing behavior was studied on blend composites having 0.75 wt% (approx. 0.43 vol%) MWCNTs, whereby the composite based on PC/PS 70/30 wt% showed the highest electrical conductivity value and the best state of macrodispersion of MWCNTs. The three kinds of CPCs exhibit different sensing behavior towards different organic vapors. Under the influence of moderate solvent vapors such as ethyl acetate and toluene, the CPC with sea-island structure showed a higher relative resistance change (R_{rel}) and poor reversibility, whereas CPCs with co-continuous structure showed a lower R_{rel} but excellent reversibility. All CPCs showed poor reversibility towards the good solvent vapor DCM due to its strong interaction with the two polymers. The CPCs sensors show an exponential relationship between R_{rel} and vapor concentration, as shown for acetone vapor. If the CPCs have been exposed to poor solvents such as cyclohexane, the PC/PS 50/50 wt% blend with 0.75 wt% has a higher R_{rel} equilibrium than the other CPCs due to the microstructural differences of the blend composites. With respect to blend structure, CPCs with co-continuous structure show better reversibility towards good vapors and higher R_{rel} towards poor vapors, which is attributed the larger blend interfaces that facilitate the sensing process. Despite the higher complexity in the context of CPC blend structures due to the different solvent reactions of both blend partners, the results indicate that conductive polymer blends are promising vapor sensors for the aim of leakage detection, especially due to their tunable blend structures.

CRediT authorship contribution statement

Yilong Li: Conceptualization, Data curation, Formal analysis, Funding acquisition, Investigation, Methodology, Visualization, Writing - original draft. **Jürgen Pionteck:** Conceptualization, Formal analysis, Methodology, Project administration, Resources, Validation, Writing - review & editing. **Petra Pötschke:** Conceptualization, Formal analysis, Methodology, Project administration, Resources, Software, Validation, Writing - review & editing. **Brigitte Voit:** Supervision.

Declaration of Competing Interest

The authors declare no conflict of interest.

Acknowledgement

The authors thank Dr. Roland Vogel for rheological measurements and Mr. Minoj Gnanaseelan for SEM studies (both IPF). Y. Li thanks the China Scholarship Council, China for its financial support (grant no. 201507040046) for his study as a PhD student at the IPF and Technische Universtät Dresden, Germany.

Data availability

The raw/processed data required to reproduce these findings cannot be shared at this time as the data also forms part of an ongoing study.

Supplementary material

The supplementary material contains a description of the measurement equipment, the estimation of MWCNT localization in PC/PS blends, additional SEM images of unfilled and filled blends, and the melt rheological characterization of the blend composites.

References

[1] J. Wang, J. Yang, N. Han, X. Zhou, S. Gong, J. Yang, et al., Highly sensitive and selective ethanol and acetone gas sensors based on modified ZnO nanomaterials, Mater. Des. 121 (2017) 69–76.
[2] S. Navale, Z. Yang, C. Liu, P. Cao, V. Patil, N. Ramgir, et al., Enhanced acetone sensing properties of titanium dioxide nanoparticles with a sub-ppm detection limit, Sensors Actuators B Chem. 255 (2018) 1701–1710.
[3] W. Li, N.-D. Hoa, Y. Cho, D. Kim, J.-S. Kim, Nanofibers of conducting polyaniline for aromatic organic compound sensor, Sensors Actuators B Chem. 143 (1) (2009) 132–138.
[4] Q. Nie, W. Zhang, L. Wang, Z. Guo, C. Li, J. Yao, et al., Sensitivity enhanced, stability improved ethanol gas sensor based on multi-wall carbon nanotubes functionalized with Pt-Pd nanoparticles, Sensors Actuators B Chem. 270 (2018) 140–148.
[5] H. Qi, J. Liu, J. Pionteck, P. Pötschke, E. Mäder, Carbon nanotube–cellulose composite aerogels for vapour sensing, Sensors Actuators B Chem. 213 (2015) 20–26.
[6] T. Villmow, A. John, P. Pötschke, G. Heinrich, Polymer/carbon nanotube composites for liquid sensing: selectivity against different solvents, Polymer 53 (14) (2012) 2908–2918.
[7] Q. Fan, Z. Qin, T. Villmow, J. Pionteck, P. Pötschke, Y. Wu, et al., Vapor sensing properties of thermoplastic polyurethane multifilament covered with carbon nanotube networks, Sensors Actuators B Chem. 156 (1) (2011) 63–70.
[8] T. Baimpos, P. Boutikos, V. Nikolakis, D. Kouzoudis, A polymer-Metglas sensor used to detect volatile organic compounds, Sensors Actuators A Phys. 158 (2) (2010) 249–253.
[9] R. Mondal, K. Dubey, Y. Bhardwaj, L. Varshney, Novel hybrid nanocarbons/poly (dimethylsiloxane) composites based chemiresistors for real time detection of hazardous aromatic hydrocarbons, Carbon 100 (2016) 42–51.
[10] M. Consales, A. Crescitelli, M. Penza, P. Aversa, P.D. Veneri, M. Giordano, et al., SWCNT nano-composite optical sensors for VOC and gas trace detection, Sensors Actuators B Chem. 138 (1) (2009) 351–361.
[11] S. Chatterjee, M. Castro, J.-F. Feller, An e-nose made of carbon nanotube based quantum resistive sensors for the detection of eighteen polar/nonpolar VOC biomarkers of lung cancer, J. Mater. Chem. B 1 (36) (2013) 4563–4575.
[12] F.J. Ibañez, F.P. Zamborini, Chemiresistive sensing of volatile organic compounds with films of surfactant-stabilized gold and gold— silver alloy nanoparticles, ACS Nano 2 (8) (2008) 1543–1552.
[13] H. Souri, D. Bhattacharyya, Wearable strain sensors based on electrically conductive natural fiber yarns, Mater. Des. 154 (2018) 217–227.
[14] Y. Liu, H. Zheng, M. Liu, High performance strain sensors based on chitosan/carbon black composite sponges, Mater. Des. 141 (2018) 276–285.
[15] S. Chen, Y. Wei, S. Wei, Y. Lin, L. Liu, Ultrasensitive cracking-assisted strain sensors based on silver nanowires/graphene hybrid particles, ACS Appl. Mater. Interfaces 8 (38) (2016) 25563–25570.
[16] K. Ke, P. Pötschke, S. Gao, B. Voit, An ionic liquid as interface linker for tuning piezoresistive sensitivity and toughness in poly (vinylidene fluoride)/carbon nanotube composites, ACS Appl. Mater. Interfaces 9 (6) (2017) 5437–5446.
[17] H. Liu, J. Gao, W. Huang, K. Dai, G. Zheng, C. Liu, et al., Electrically conductive strain sensing polyurethane nanocomposites with synergistic carbon nanotubes and graphene bifillers, Nanoscale 8 (26) (2016) 12977–12989.
[18] Y. Li, H. Liu, K. Dai, G. Zheng, C. Liu, J. Chen, et al., Tuning of vapor sensing behaviors of eco-friendly conductive polymer composites utilizing ramie fiber, Sensors Actuators B Chem. 221 (2015) 1279–1289.
[19] J. Tabačiarová, J. Krajči, J. Pionteck, U. Reuter, M. Omastová, M. Mičušík, Styrene butadiene rubber/carbon filler-based vapor sensors, Macromol. Chem. Phys. 217 (10) (2016) 1149–1160.
[20] S.P. Pawar, D.A. Marathe, K. Pattabhi, S. Bose, Electromagnetic interference shielding through MWNT grafted Fe 3 O 4 nanoparticles in PC/SAN blends, J. Mater. Chem. A 3 (2) (2015) 656–669.
[21] S.P. Pawar, S. Stephen, S. Bose, V. Mittal, Tailored electrical conductivity, electromagnetic shielding and thermal transport in polymeric blends with graphene sheets decorated with nickel nanoparticles, Phys. Chem. Chem. Phys. 17 (22) (2015) 14922–14930.
[22] D.-X. Yan, P.-G. Ren, H. Pang, Q. Fu, M.-B. Yang, Z.-M. Li, Efficient electromagnetic interference shielding of lightweight graphene/polystyrene composite, J. Mater. Chem. 22 (36) (2012) 18772–18774.
[23] Y. Xu, S. Tang, J. Pan, J. Bao, A. Zhang, Reversibly cross-linked SEBS/carbon hybrid composite with excellent solvent-proof and electromagnetic shielding properties, Mater. Des. 146 (2018) 1–11.
[24] B. Ding, M. Wang, X. Wang, J. Yu, G. Sun, Electrospun nanomaterials for ultrasensitive sensors, Mater. Today 13 (11) (2010) 16–27.
[25] J. Feller, Y. Grohens, Electrical response of poly (styrene)/carbon black conductive polymer composites (CPC) to methanol, toluene, chloroform and styrene vapors as a function of filler nature and matrix tacticity, Synth. Met. 154 (1–3) (2005) 193–196.
[26] A. Daneshkhah, S. Shrestha, M. Agarwal, K. Varahramyan, Poly (vinylidene fluoride-hexafluoropropylene) composite sensors for volatile organic compounds detection in breath, Sensors Actuators B Chem. 221 (2015) 635–643.
[27] B. Kumar, M. Castro, J.-F. Feller, Poly (lactic acid)–multi-wall carbon nanotube conductive biopolymer nanocomposite vapour sensors, Sensors Actuators B Chem. 161 (1) (2012) 621–628.
[28] B. Kumar, M. Castro, J.-F. Feller, Controlled conductive junction gap for chitosan–carbon nanotube quantum resistive vapour sensors, J. Mater. Chem. 22 (21) (2012) 10656–10664.
[29] J. Lu, B. Kumar, M. Castro, J.-F. Feller, Vapour sensing with conductive polymer nanocomposites (CPC): polycarbonate-carbon nanotubes transducers with hierarchical structure processed by spray layer by layer, Sensors Actuators B Chem. 140 (2) (2009) 451–460.
[30] B. Kumar, J.-F. Feller, M. Castro, J. Lu, Conductive bio-Polymer nano-Composites (CPC): chitosan-carbon nanotube transducers assembled via spray layer-by-layer for volatile organic compound sensing, Talanta 81 (3) (2010) 908–915.
[31] Y. Chen, P. Pötschke, J. Pionteck, B. Voit, H. Qi, Smart cellulose/graphene composites fabricated by in situ chemical reduction of graphene oxide for multiple sensing applications, J. Mater. Chem. A 6 (17) (2018) 7777–7785.
[32] Y. Li, P. Pötschke, J. Pionteck, B. Voit, Electrical and vapor sensing behaviors of polycarbonate composites containing hybrid carbon fillers, Eur. Polym. J. 108 (2018) 461–471.
[33] M. Moniruzzaman, K.I. Winey, Polymer nanocomposites containing carbon nanotubes, Macromolecules 39 (16) (2006) 5194–5205.
[34] M.H. Al-Saleh, H.K. Al-Anid, Y.A. Hussain, Electrical double percolation and carbon nanotubes distribution in solution processed immiscible polymer blend, Synth. Met. 175 (2013) 75–80.
[35] B. Arash, Q. Wang, V. Varadan, Mechanical properties of carbon nanotube/polymer composites, Sci. Rep. 4 (2014) 6479.
[36] H. Liu, Y. Li, K. Dai, G. Zheng, C. Liu, C. Shen, et al., Electrically conductive thermoplastic elastomer nanocomposites at ultralow graphene loading levels for strain sensor applications, J. Mater. Chem. C 4 (1) (2016) 157–166.
[37] J. Chen, X. Cui, Y. Zhu, W. Jiang, K. Sui, Design of superior conductive polymer composite with precisely controlling carbon nanotubes at the interface of a co-continuous polymer blend via a balance of π-π interactions and dipole-dipole interactions, Carbon 114 (2017) 441–448.
[38] J. Chen, X. Cui, K. Sui, Y. Zhu, W. Jiang, Balance the electrical properties and mechanical properties of carbon black filled immiscible polymer blends with a double percolation structure, Compos. Sci. Technol. 140 (2017) 99–105.
[39] C. Roman, M. García-Morales, J. Gupta, T. McNally, On the phase affinity of multi-walled carbon nanotubes in PMMA: LDPE immiscible polymer blends, Polymer 118 (2017) 1–11.
[40] A.H.A. Hoseini, M. Arjmand, U. Sundararaj, M. Trifkovic, Tunable electrical conductivity of polystyrene/polyamide-6/carbon nanotube blend nanocomposites via control of morphology and nanofiller localization, Eur. Polym. J. 95 (2017) 418–429.
[41] Y. Li, Y. Zheng, P. Zhan, G. Zheng, K. Dai, C. Liu, et al., Vapor sensing performance as a diagnosis probe to estimate the distribution of multi-walled carbon nanotubes in poly (lactic acid)/polypropylene conductive composites, Sensors Actuators B Chem. 255 (2018) 2809–2819.
[42] J. Gao, H. Wang, X. Huang, M. Hu, H. Xue, R.K. Li, A super-hydrophobic and electrically conductive nanofibrous membrane for a chemical vapor sensor, J. Mater. Chem. A 6 (21) (2018) 10036–10047.
[43] R. Arrigo, N.T. Dintcheva, E. Morici, F.P. La Mantia, Performances and morphology of polyamide/carbonaceous structures based fibers, AIP Conference Proceedings, vol. 1599, 2014, pp. 330–333.
[44] B. Krause, M. Mende, P. Pötschke, G. Petzold, Dispersability and particle size distribution of CNTs in an aqueous surfactant dispersion as a function of ultrasonic treatment time, Carbon 48 (10) (2010) 2746–2754.
[45] I. Alig, P. Pötschke, D. Lellinger, T. Skipa, S. Pegel, G.R. Kasaliwal, et al., Establishment, morphology and properties of carbon nanotube networks in polymer melts, Polymer 53 (1) (2012) 4–28.
[46] J.A. Galloway, K.J. Koester, B.J. Paasch, C.W. Macosko, Effect of sample size on solvent extraction for detecting cocontinuity in polymer blends, Polymer 45 (2) (2004) 423–428.
[47] P. Pötschke, D. Paul, Formation of co-continuous structures in melt-mixed immiscible polymer blends, J. Macromol. Sci. Polym. Rev. 43 (1) (2003) 87–141.
[48] K. Kobashi, T. Villmow, T. Andres, L. Häußler, P. Pötschke, Investigation of liquid sensing mechanism of poly (lactic acid)/multi-walled carbon nanotube composite films, Smart Mater. Struct. 18 (3) (2009), 035008.
[49] A. Bouvree, J.-F. Feller, M. Castro, Y. Grohens, M. Rinaudo, Conductive polymer nanobiocomposites (CPC): chitosan-carbon nanoparticle a good candidate to design polar vapour sensors, Sensors Actuators B Chem. 138 (1) (2009) 138–147.
[50] C.M. Hansen, Hansen Solubility Parameters: A user's Handbook, CRC press, 2007.